



# Firm mantle plumes and the nature of the core–mantle boundary region

Jun Korenaga\*

*Department of Geology and Geophysics, Yale University, P.O. Box 208109, New Haven, CT 06520-8109, USA*

Received 9 September 2004; received in revised form 22 December 2004; accepted 6 January 2005

Editor: S. King

## Abstract

Recent tomographic imaging of thick plume conduits in the lower mantle, when combined with plume buoyancy flux based on hotspot swell topography, indicates a very high plume viscosity of  $10^{21}$ – $10^{23}$  Pa s. This estimated plume viscosity is comparable or may even be greater than the viscosity of the bulk lower mantle, the estimate of which ranges from  $2 \times 10^{21}$  to  $10^{22}$  Pa s. Here I show that both very high viscosity and large radii of lower-mantle plumes can be simultaneously explained if the temperature dependency of lower-mantle rheology is dominated by the grain size-dependent part of diffusion creep, i.e., hotter mantle has higher viscosity. Fluid-dynamical scaling laws of a thermal boundary layer suggest that the thickness and topography of the  $D''$  discontinuity are consistent with such mantle rheology. This new kind of plume dynamics may also explain why plumes appear to be fixed in space despite background mantle flow and why plume excess temperature is only up to 200–300 K whereas the temperature difference at the core–mantle boundary is likely to exceed 1000 K.

© 2005 Elsevier B.V. All rights reserved.

*Keywords:* mantle plumes; seismic tomography; hotspot swells; diffusion creep; grain growth

## 1. Introduction

Seismic imaging of deep mantle plumes has long been considered as a daunting task [1] because plume conduits are believed to be a narrow feature with a radius of much less than 100 km [2,3] and the wave front healing effect makes such a small-scale feature

almost invisible [4]. Traditionally, the Rayleigh–Taylor instability of a hot bottom boundary layer is thought to produce the upwelling of a less viscous plume through a more viscous overlying fluid. Viscosity contrast between a plume and the ambient mantle is typically assumed to be on the order of  $10^2$ – $10^3$ , and this contrast results in the formation of a large spherical head followed by a narrow conduit (Fig. 1). It is thus quite surprising that a recent finite-frequency tomography has resolved quite a few deep mantle plumes with very large radii, typically ranging

\* Tel.: +1 203 432 7381; fax: +1 203 432 3134.

E-mail address: [jun.korenaga@yale.edu](mailto:jun.korenaga@yale.edu).

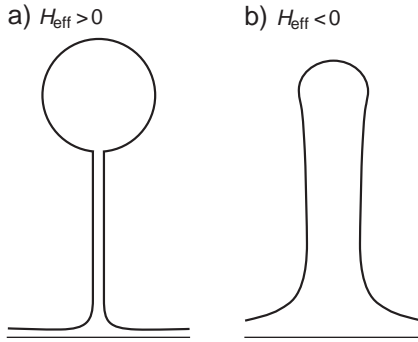


Fig. 1. The different sign of the activation enthalpy results in different plume morphology and dynamics [2,19,30]. (a) In the case of positive activation enthalpy, a less viscous plume rises through a more viscous fluid. A large spherical head forms followed by a narrow plume conduit. (b) Negative activation enthalpy results in a more viscous plume intruding in a less viscous fluid. Plume head and tail have similar radii, and upwelling is more diffuse.

from 200 to 400 km [5]. The lateral dimension of those imaged plumes is one of the most reliable features of the tomography. The reported radii are the minimum estimate based on extensive resolution tests (note: the tomographic images presented by [5] generally show larger radii than these minimum estimates because of blurring inherent in tomography); if plume conduits are narrower, even finite-frequency tomography could not image them. Although it is sometimes claimed that recent dynamic models exhibit similarly thick plumes [6], those plumes with large radii result from the use of temperature-independent viscosity and/or low Rayleigh number (i.e., very high mantle viscosity) in numerical modeling. As I will demonstrate in the following, thick plume conduits, whether created in numerical models or imaged in seismic tomography, imply a serious conflict with the surface observation of plume flux, if dynamics is properly scaled to the Earth's mantle and if plume viscosity is assumed to be lower than the surrounding mantle. The seismically imaged thick conduits, if they are indeed a solid feature as claimed by [5], may require a fundamental rethinking of plume dynamics.

## 2. Plume buoyancy flux and plume radius

Plume buoyancy flux [7] provides a robust constraint on the flux of hot material brought to the near

surface by a plume. The buoyancy flux is calculated from swell excess topography, absolute plate velocity, and density contrast between mantle and seawater, all of which are known with reasonable accuracy. Hawaii has by far the largest buoyancy flux of  $8700 \text{ kg s}^{-1}$ ; other hotspots mostly fall in the range of  $1000\text{--}4000 \text{ kg s}^{-1}$  [7]. These estimates are most likely the upper bound for thermal buoyancy flux because not all of swell topography can be attributed to the thermal buoyancy of mantle plumes. Dynamic tomography due to viscous stress [8] as well as compositional buoyancy resulting from mantle melting [9] may reduce the estimated flux. In addition, small-scale convection may facilitate the thinning of lithosphere [10], either independently of or coupled with plume influx. It is important to note that this upper bound on plume flux corresponds to the lower bound on plume viscosity estimated in the following, thus making my argument robust.

The plume buoyancy flux,  $\dot{M}_A$ , is related to the plume heat flux,  $Q$ , as  $\dot{M}_A = \alpha^U Q / c_p^U$ , where  $\alpha$  is thermal expansivity,  $c_p$  is specific heat at constant pressure, and the superscript U indicates the upper mantle values appropriate for surface expression like swell topography. Assuming steady state, buoyancy-driven axisymmetric upwelling through a circular conduit, then, the buoyancy flux of a plume and its conduit radius ( $a$ ) may be related as [3]:

$$\dot{M}_A = \frac{\pi(\alpha\rho_0\Delta T_p)^2 g a^4}{A\mu_p} \quad (1)$$

where  $\rho_0$  is reference density,  $\Delta T_p$  is the amplitude of plume temperature anomaly,  $g$  is gravitational acceleration, and  $\mu_p$  is centerline plume viscosity (much lower than ambient viscosity,  $\mu_0$ , owing to temperature-dependent viscosity). In the numerical and theoretical models of [3], linear exponential viscosity is employed with a parabolic temperature distribution. The total viscosity contrast is given by  $\varepsilon \equiv \mu_0/\mu_p$ , and Eq. (1) is valid only when  $\varepsilon \gg 1$  ( $\varepsilon$  is typically  $10^2\text{--}10^3$  in previous studies). The constant  $A$  is equal to  $(\alpha/\alpha^U)(c_p^U/c_p)(\log(\varepsilon))^2$ . The conduit radius is defined here as the radius where the temperature anomaly is one-half its centerline value [3], thus the radius  $a$  covers the dominant part of the thermal halo. Note that, because viscosity is much lower at the center of the plume conduit, the mechanical conduit is much

narrower than this thermal halo. What is most relevant to seismic tomography is the thermal halo, and the definition of the radius  $a$  here approximately corresponds to the definition of plume radius adopted by [5] (where seismic velocity anomaly drops less than 0.3%, corresponding to the temperature anomaly of 100 K in the lower mantle).

The most uncertain parameter here is plume viscosity, which can vary by a few orders of magnitudes; the uncertainty of other parameters is less than a factor of two. This scaling law is compared to the observed correlation between plume flux and radius in Fig. 2, which suggests that plume viscosity is likely to be greater than  $10^{21}$  Pa s for most of deep-mantle plumes and can be as high as  $10^{23}$  Pa s in some cases. In most of previous studies on plume dynamics, plume viscosity has been assumed to be much lower, typically around  $10^{19}$  Pa s. With such a low viscosity, the thick plume conduits as inferred from the finite-frequency tomography would produce an unacceptably high plume flux of  $10^5$ – $10^6$  kg s<sup>-1</sup> because the buoyancy flux by Poiseuille-type flow is proportional to the fourth power of the conduit radius (Eq. (1)). As

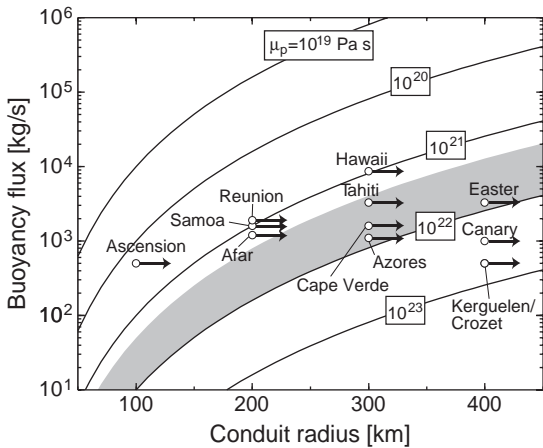


Fig. 2. Correlation of plume radius [5] and plume buoyancy flux [7]. Only plumes originating in the vicinity of the D'' layer, as reported by [5], are considered here, including three likely members (Hawaii, Afar, and Reunion). Horizontal arrows are used to emphasize that the reported radius is the minimum estimate. Curves denote the prediction of Eq. (1) with mid-mantle values,  $\alpha=10^{-5}$  K<sup>-1</sup> [38],  $\rho_0=5000$  kg m<sup>-3</sup> [39],  $g=10$  m s<sup>-2</sup>,  $\Delta T_p=300$  K, and plume viscosity ranging from  $10^{19}$  Pa s to  $10^{23}$  Pa s. Following values are used for the constant  $A$ ;  $\alpha^U=3 \times 10^{-5}$  K<sup>-1</sup>,  $c_p^U/c_p=1$ , and  $\varepsilon=100$ . Shaded region corresponds to the range of estimated lower-mantle viscosity [11].

far as hotspot swells are regarded as the surface expression of imaged mantle plumes, therefore, high plume viscosity appears to be an inevitable geodynamical interpretation of the tomography. One may argue that plume flux may actually be highly time-dependent and the assumption of steady-state dynamics in Eq. (1) is inappropriate. It is highly unlikely, however, that all of deep mantle plumes are synchronously in a reduced flux state. Moreover, time-dependent behavior (e.g., starting plume) tends to give rise to greater flux than the steady state [6], so the use of steady-state formula corresponds to the lower bound on plume viscosity. It should be noted that, with this approach, heat flux carried by mantle plumes remains essentially the same as that estimated by Sleep [7], i.e.,  $\sim 2$  TW. Although Montelli et al. [5] argued that their tomographic image indicates much larger plume heat flux than previously estimated, seeing large radii does not readily imply high heat flux because seismic image alone cannot constrain plume rise velocities.

The inferred plume viscosity,  $10^{21}$ – $10^{23}$  Pa s, is comparable to or may exceed the viscosity of bulk lower mantle ( $\mu_{LM}$ ), the estimate of which ranges from  $2 \times 10^{21}$ – $10^{22}$  Pa s [11]. For the above assumption of Poiseuille-type flow to be valid, plume must be much less viscous than the surrounding mantle, which acts as a rigid wall. This restriction to the classical Poiseuille flow can be relaxed by considering a more general case of buoyant axisymmetric upwelling, in which a plume conduit with radius  $a$  and viscosity  $\mu_p$  is surrounded by a medium with radius  $b(>a)$  and viscosity  $\mu_0$ . Assuming lithostatic pressure gradient and zero radial velocity, upwelling velocity may be expressed as

$$U_1(r) = \frac{\Delta \rho g a^2}{4 \mu_p} \left[ 1 - \left( \frac{r}{a} \right)^2 - \frac{2 \ln f}{\varepsilon} \right] \quad (0 \leq r \leq a) \quad (2)$$

$$U_2(r) = - \frac{\Delta \rho g a^2}{2 \varepsilon \mu_p} \ln \left( \frac{r}{b} \right) \quad (a < r \leq b) \quad (3)$$

where density difference between the plume and the surrounding is denoted as  $\Delta \rho$  ( $\equiv \alpha \rho_0 \Delta T_0$ ) and  $f=a/b$ . The derivation of this solution is elementary; it can easily be verified that the above velocity field satisfies the Stokes equation with continuous velocity and

traction at  $r=a$  and vanishing velocity at  $r=b$ . Corresponding buoyancy flux is then

$$\dot{M}_B = \frac{\pi(\alpha\rho_0\Delta T_0)^2 g a^4}{B\mu_p}, \quad (4)$$

where

$$B = \left(\frac{\alpha}{\alpha^U}\right) \left(\frac{c_p^U}{c_p}\right) \left(\frac{8\varepsilon}{\varepsilon - 4\ln f}\right). \quad (5)$$

When the plume viscosity is comparable with the ambient viscosity,  $\varepsilon$  is on the order of 1. Since the spacing of deep mantle plumes is typically on the order of 1000–2000 km [5], a reasonable range for  $f$  would be 0.2–0.5, which indicates that the scaling factor  $B$  is smaller than  $A$  by one order of magnitude. The estimate of plume viscosity based on the low-viscosity Poiseuille flow assumption (Fig. 2) is therefore the lower bound. Plume viscosity is likely to be equal to or greater than the viscosity of the ambient lower mantle, and there are in total three reasons to make this inference robust: (1) Montelli et al. [5] provide the lower bound on plume radius, (2) Sleep [7] provides the upper bound on plume flux, and (3) the assumption of steady-state Poiseuille-type flow in Eq. (1) gives rise to the lower bound on plume viscosity.

### 3. Hotter, stiffer plumes?

One way to understand the inferred relation between the viscosities of plumes and of the surrounding mantle is to assume that the effective activation enthalpy is negative, i.e., hotter mantle becomes more viscous. This may sound counter-intuitive, but it has been suggested to be physically plausible when mantle deformation is controlled by diffusion creep [12]. Diffusion creep is very sensitive to grain size,  $d$ , as well as temperature,  $T$ , as

$$\mu \propto d^m \exp(H_d/RT), \quad (6)$$

where  $m$  is a constant ( $\sim 3$ ),  $H_d$  is the activation enthalpy for diffusion creep, and  $R$  is the universal gas constant. On the other hand, grains grow faster in a hotter environment as indicated by

$$d^m - d_0^m \propto t \exp(-H_g/RT), \quad (7)$$

where  $n$  is a constant (typically around 2–3 [13]),  $d_0$  is the initial grain size,  $t$  is time, and  $H_g$  is the activation enthalpy for grain growth. The effective activation enthalpy for grain size-sensitive diffusion creep is therefore given by

$$H_{\text{eff}} = H_d - \frac{m}{n} H_g. \quad (8)$$

Although the number of experimental studies has steadily been growing [14,15], the rheology of lower-mantle minerals and their aggregates, including the dynamics of grain growth, is yet to be known in details. Solomatov [12,16] argues that the effective activation enthalpy can take any value including negative. At this point, therefore, it appears reasonable to take  $H_{\text{eff}}$  as a free parameter and to test if a non-positive activation enthalpy can reproduce geophysical observations on the basis of fluid-dynamical scaling laws.

The dynamics of a hot, bottom boundary layer with a negative activation enthalpy is exactly the same as that of a cold, top boundary layer with a positive activation enthalpy. The latter has been studied extensively in relation to small-scale convection in the upper mantle [17–20]. Viscosity variation in the bottom boundary layer may be described by the following nondimensionalized Arrhenius form:

$$\mu^* = \exp\left(\frac{H^*}{T^* + T_{\text{off}}^*} - \frac{H^*}{T_{\text{off}}^*}\right), \quad (9)$$

where  $H^* = H_{\text{eff}}/(R\Delta T)$ ,  $T_{\text{off}}^* > T_0/\Delta T$ ,  $\Delta T$  is the temperature contrast across the boundary layer ( $\sim 1000$ – $2000$  K [21]), and  $T_0$  is the mantle temperature right above the boundary layer ( $\sim 3000$  K [22]). Viscosity is normalized by  $\mu_{\text{LM}}$ , the viscosity of the lower mantle at  $T=T_0$ . The normalized temperature,  $T^*$ , varies from 0 (top) to 1 (bottom) in the boundary layer. To measure the degree of temperature dependency, it is convenient to introduce the Frank–Kamenetskii parameter,  $\sigma$ , which is defined as

$$\sigma = - \left. \frac{d \log \mu^*}{dT^*} \right|_{T^*=0} = \frac{-H_{\text{eff}} \Delta T}{RT_0^2}. \quad (10)$$

An isoviscous case corresponds to  $\sigma=0$ , and roughly speaking, a nondimensional temperature change of  $\sigma^{-1}$  yields a change in viscosity by a factor of  $e$ . Under the transformation from  $T^*$  to  $1-T^*$ , the problem of the bottom boundary layer becomes

mathematically identical to that of the top boundary layer. There are, however, two important differences. First, the Arrhenius viscosity results in a sub-exponential, rather than super-exponential, variation of viscosity across the boundary layer. Second, the high reference temperature gives rise to a weak temperature sensitivity; with  $\Delta T=1000$  K, for example,  $\sigma$  is only  $\sim 4$  even when  $H_{\text{eff}}$  is as low as  $-300$  kJ mol $^{-1}$  (cf.  $\sigma\sim 8$  with  $\Delta T=2000$  K). For this small range of  $\sigma$ , it is important to take into account the exact form of temperature dependency (e.g., Arrhenius or exponential) for accurate evaluation of convective instability [19].

The bottom thermal boundary layer grows as it receives heat from the core and eventually starts to convect when its local Rayleigh number exceeds a critical value [19]. With a negative activation enthalpy, the hottest part of the boundary layer does not participate in this convective instability because of its high viscosity. Only some top fraction of the boundary layer, which is less viscous and thus mobile enough, can delaminate and evolve into an upwelling plume. This physics of the onset of convection, i.e., transition from infinitesimal perturbations to finite amplitude convection, is most likely dominated by diffusion creep. Non-Newtonian rheology cannot be an efficient deformation mechanism because of its virtually infinite effective viscosity at such transition.

With  $H_g$  of a few hundred kJ mol $^{-1}$ , the time scale of grain growth is similar to that of boundary layer growth; a slight delay in grain growth can be modeled as an apparent increase in activation energy as shown below. The grain growth equation (Eq. (7)) may be arranged into a differential form:

$$\frac{d(d^m(t))}{dt} = D e^{-H_g/RT}, \quad (11)$$

where  $D$  is a scaling constant. When temperature  $T$  changes from  $T_0$  to  $T_0+\Delta T$  by the growth of a thermal boundary layer, one can integrate the above equation to obtain the grain growth curve. Let us denote this growth curve by  $d_1(t)$  and the time scale of this temperature change by  $\tau_d$ . On the other hand, “instantaneous” adjustment of grain size to the final temperature  $T_0+\Delta T$ , which is implicit in my treatment of the onset of convection, can be expressed as

$$d_2(t)^n - d_2(0)^n = D t e^{-H_g/R(T_0+\Delta T)}. \quad (12)$$

When  $e^{-H_g/RT_0}$  is negligible compared to  $e^{-H_g/R(T_0+\Delta T)}$ , difference between  $d_1(t)$  and  $d_2(t)$  can be approximated as

$$\frac{d_2^n - d_1^n}{d_2^n} \sim \frac{\tau_d}{2t}. \quad (13)$$

That is, when temperature change is just completed ( $t=\tau_d$ ),  $d_1$  is about 70–80% of  $d_2$  (assuming  $n=2-3$ ), and this difference will gradually diminish as  $t$  increases further. Since  $d^n$  is proportional to  $e^{-H_g/RT}$ , this difference may be translated as an error in activation energy,  $\Delta H \sim RT \log 2$ , which is only a few percents of  $H_g$ .

The critical thickness of the boundary layer at the onset of convection, the thickness of the mobile sublayer, and the temperature drop across the sublayer can all be predicted as a function of the Frank–Kamenetskii parameter, on the basis of recently developed scaling laws on convective instability [19,20] (Fig. 3). Although similar scaling laws have recently been published [23,24], the scaling law of Korenaga and Jordan [19] is the only one that can handle from constant viscosity to strongly temperature-dependent viscosity as well as sub-exponential temperature dependency, both of which are important to the present problem as already noted. Such predictions can be compared with the thickness of the  $D'$  layer, its topography, and the excess temperature of mantle plumes, respectively. The primary sources of uncertainty in this prediction are the total temperature difference across the boundary layer  $\Delta T$  and the reference lower-mantle viscosity  $\mu_{\text{LM}}$ . The viscosity and temperature contrasts in the delaminated mobile sublayer are insensitive to the assumed reference viscosity, whereas the boundary layer thickness is affected by both parameters. I take  $\Delta T=1000$  K and  $\mu_{\text{LM}}=2 \times 10^{21}$  Pa s as the standard case and show the range of uncertainty by changing  $\Delta T$  to 2000 K and  $\mu_{\text{LM}}$  to  $10^{22}$  Pa s.

The temperature contrast in the mobile sublayer is only a fraction of  $\Delta T$  (Fig. 3b), and it can be used as the upper bound on plume excess temperature. As discussed later, this temperature contrast could further decrease considerably during the ascent of a plume by thermal diffusion. The partial delamination of the boundary layer combined with subsequent diffusional heat loss, therefore, may explain why the petrological estimate of plume excess temperature is only 100–300

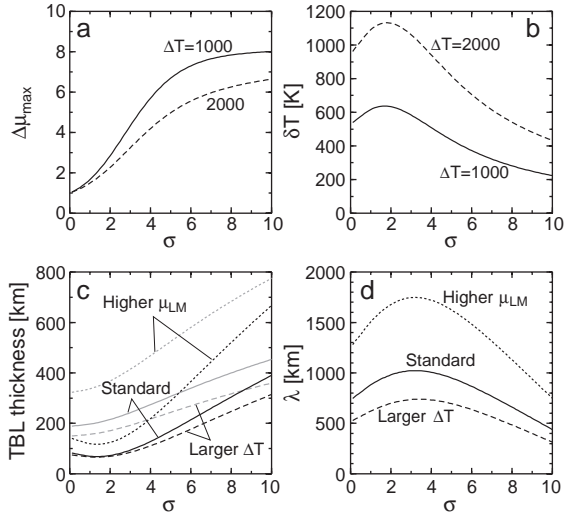


Fig. 3. Characteristics of boundary layer as a function of the Frank–Kamenetskii parameter  $\sigma$  based on scaling laws of [19] with the correction of 60% maximum viscosity as suggested by [20]. The critical Rayleigh number is set to 1300. Other relevant physical parameters are set to lowermost-mantle values:  $\alpha=10^{-5} \text{ K}^{-1}$ ,  $\rho_0=5500 \text{ kg m}^{-3}$ ,  $g=10 \text{ m s}^{-2}$ , and  $\kappa=10^{-6} \text{ m}^2 \text{ s}^{-1}$ . (a) Viscosity contrast and (b) temperature contrast across the mobile sublayer. Solid and dashed lines correspond to  $\Delta T=1000 \text{ K}$  and  $\Delta T=2000 \text{ K}$ , respectively. (c) Boundary layer thicknesses at and after the onset of convection are denoted by black and gray lines, respectively. Solid curves show the standard case ( $\mu_{\text{LM}}=2 \times 10^{21} \text{ Pa s}$  and  $\Delta T=1000 \text{ K}$ ). Dashed curves are for  $\Delta T=2000 \text{ K}$  with the standard viscosity, and dotted curves for  $\mu_{\text{LM}}=10^{22} \text{ Pa s}$  with the standard temperature difference. (d) Wavelength with the maximum growth rate for the Rayleigh–Taylor instability [30]. Density difference is given by  $\alpha\rho_0\delta T$ . Layer thickness is simply the thickness of the mobile layer. Viscosity contrast is given by the logarithmic average of the minimum and maximum viscosity attained in the mobile sublayer, i.e.,  $\sqrt{\Delta\mu_{\text{max}}}$ . Legend is the same as in panel (c).

K [25], whereas the temperature contrast expected at the core–mantle boundary is on the order of 1000 K. Farnetani [26] attempted to resolve this apparent paradox by introducing a dense chemical layer above the core–mantle boundary, which tends to suppress the convective instability of the thermal boundary layer. Although there are ample evidence for a chemically heterogeneous lowermost mantle [27,28], the material properties of such heterogeneity are still uncertain and the range of possible dynamics is quite large [29]. Even if chemical heterogeneity does not play the required dynamical role, however, the present study suggests that the temperature paradox may also be resolved by a negative activation enthalpy.

The thicknesses of the boundary layer at and after the onset of convective instability are on the order of a few hundred kilometers for a range of  $\sigma$  (Fig. 3c), which compares well with the thickness of the D'' layer [27]. After the onset of convection, the boundary layer thickness is reduced by the delamination of the mobile sublayer. Thus, if the D'' layer is a thermal boundary layer, its variation in thickness is essentially determined by the thickness of the mobile sublayer. Fig. 3c shows that the thickness of the mobile part is  $\sim 100\text{--}200 \text{ km}$ , which is comparable with the topography of the D'' discontinuity [28]. Furthermore, the wavelength of the most unstable perturbation can also be predicted based on the theory of the Rayleigh–Taylor instability [30], using the above predicted feature of the mobile sublayer. The predicted wavelength of  $\sim 1000\text{--}2000 \text{ km}$  (Fig. 3d) is in accord with the spacing of seismically imaged mantle plumes at the core–mantle boundary [5]. Given the uncertainty involved in  $\Delta T$  and  $\mu_{\text{LM}}$ , it is difficult to narrow down the likely range of  $\sigma$  with confidence. Even the case of  $\sigma=0$  (zero activation enthalpy) is possible with higher  $\mu_{\text{LM}}$  and lower  $\Delta T$  (Fig. 3); the lower mantle could be nearly isoviscous regardless of temperature variations.

#### 4. Discussion and conclusion

The morphology of seismically imaged plumes, including those which have not reached the surface yet [5], appears to be more similar to viscous plumes intruding less viscous fluid than to less viscous plumes intruding more viscous fluid (see Fig. 1 of [30]). Although fast-moving spherical plume heads are often invoked to explain the formation of large igneous provinces [2], such geological inference remains speculative. Indeed, the origin of continental breakup magmatism, for example, does not seem to be consistent with the notion of a plume head impact; a recent study suggests that such massive magmatism may be better explained by intrinsic chemical anomalies in the mantle [31]. Since average upwelling velocity is given by  $\dot{M}/(\pi a^2 \Delta\rho^{\text{U}})$ , a larger plume radius means slower upwelling. For the 12 deep plumes considered here, average  $\dot{M}$  is  $\sim 2000 \text{ kg s}^{-1}$  [7] and average radius is  $\sim 300 \text{ km}$ , which translates to a typical upwelling velocity of  $\sim 1 \text{ cm yr}^{-1}$ . Thus, it may take  $\sim 300 \text{ m.y.}$  for a plume to

travel from the core–mantle boundary to the surface, so the effect of thermal diffusion is obviously a concern. An appropriate diffusion time scale is  $\tau_d = r_0^2 / (4\kappa)$  [32], where  $\kappa$  is thermal diffusivity and  $r_0$  is the initial plume radius at the base of the mantle. Over this time scale, the center temperature of a plume decreases by a factor of 2, whereas the plume radius could increase by a factor of up to  $\sqrt{2}$ , depending on how the ambient mantle interacts with this slowly moving plume. For  $r_0 = 200$ – $300$  km,  $\tau_d \sim 300$ – $700$  m.y., which is comparable with the time scale of plume ascent. Thus, plume excess temperature is likely to be in the range of 100–300 K if  $\Delta T \sim 1000$  K; that is, for the temperature difference of 1000 K at the core–mantle boundary, only 200–600 K can be incorporated into convective upwelling because of a hot and stiff boundary layer (Fig. 3b), and then because of slow upwelling, the excess temperature further reduces by a factor of 2 owing to thermal diffusion. Thanks to a large radius, a plume would not diffuse away although it rises very slowly.

Another concern is how to explain the spatial fixity of such slow-moving plumes since many hotspots appear to be more or less fixed in the absolute plate motion frame [33,34]. A negative activation enthalpy offers two mechanisms that could potentially explain the stability of upwelling plumes. First of all, the lower portion of the  $D''$  layer is more viscous than the bulk lower mantle, so the topography of the  $D''$  layer, once formed by the formation of upwelling plumes, tends to remain intact. This topography may serve to anchor the location of upwelling. Although stress is generally high in the boundary layer, negligible strain rate (at least initially owing to large grain sizes) may inhibit transition to dislocation creep, the activation of which requires some critical finite strain. Second, when plume viscosity is comparable with the ambient viscosity, the surrounding mantle, which itself has no thermal buoyancy, is strongly dragged by buoyant pipe flow (Eqs. (2) and (3)). The ratio of volume flux in the surrounding mantle with respect to the internal plume flux is given by

$$\frac{F_2}{F_1} = \frac{2(1 - f^2 + 2f^2 \ln f)}{f^2(\varepsilon - \ln f)}. \quad (14)$$

Note that only  $F_1$  is associated with positive temperature anomaly and thus can be observed by swell

topography ( $\dot{M} = F_1 \Delta \rho^U$ ). For  $\varepsilon \sim 1$  and  $f = 0.2$ – $0.5$ , the total upwelling volume ( $F_1 + F_2$ ) is larger than  $F_1$  by a factor of  $\sim 2$ – $6$  (Eq. (14)). The sum of the twelve plume volume fluxes is  $\sim 1300 \text{ m}^3 \text{ s}^{-1}$ , so the total upwelling flux can be up to  $2600$ – $7800 \text{ m}^3 \text{ s}^{-1}$ , which would then constitute a considerable fraction of “minimum” mantle return flow corresponding to plate subduction ( $\sim 8000 \text{ m}^3 \text{ s}^{-1}$  assuming average 75-km-thick slab [35]; slab entrainment could substantially increase material influx by subduction, but how much is highly model-dependent). Background mantle circulation, often called mantle wind, may thus be weak in the first place and have little influence on plume ascent in the lower mantle.

Firm mantle plumes indicate small lateral variation in viscosity, thus radially symmetric viscosity usually assumed in the theoretical prediction of Earth’s geoid may not be a poor approximation after all. When the lower mantle is more viscous than the upper mantle, it is possible to have a positive geoid response for positive density anomaly in the upper mantle as well as negative density anomaly in the lower mantle [36]. This may explain the general presence of geoid highs above subducted slabs and hotspots. Future efforts on interpreting hotspot geoid signature in light of this new plume dynamics may provide valuable observational constraints.

In this study, the treatment of lower-mantle rheology is designed to be simple to focus on the role of a negative activation enthalpy in boundary layer dynamics. Neglecting the  $t$  factor in Eq. (7) is probably a reasonable approximation because the time scale of convection in the lower mantle is similar to that of the growth of the  $D''$  layer (a few hundred million years); the viscosity of the ambient lower mantle should be lower than that of the hot core–mantle boundary region as far as diffusion creep is concerned. Realistic mantle rheology is of course expected to be more complex, involving both diffusion and dislocation creep [37]. Strong seismic anisotropy inferred near the core–mantle boundary [27,28] may result from dislocation creep of subducting slabs. On the other hand, the majority of the lower mantle is almost completely isotropic, which suggests the dominant deformation mechanism of diffusion creep. Lower-mantle rheology may always stay close to the transition between dislocation and diffusion creep, although it may be implausible to expect

dislocation creep in a hot stagnant lid at the bottom of the mantle because of diminishing strain rate there. Fully dynamic calculations properly incorporating the microscopic physics of grain growth are much desired to explore the possible rheological states of the lower mantle. Such study should also be able to address the fate of a deep-mantle plume entering the upper mantle. It remains to be seen how plume flux in the upper mantle is regulated by deep-mantle dynamics.

### Acknowledgments

This work has benefited from constructive discussions with Guust Nolet, Shun-ichiro Karato, and Dave Bercovici. The author also thanks thoughtful reviews by Slava Solomatov, Garrett Ito, and an anonymous reviewer.

### References

- [1] H.-C. Nataf, J. VanDecar, Seismological detection of a mantle plume? *Nature* 364 (1993) 115–120.
- [2] M.A. Richards, R.A. Duncan, V.E. Courtillot, Flood basalts and hot-spot tracks: plume heads and tails, *Science* 246 (1989) 103–107.
- [3] P. Olson, G. Schubert, C. Anderson, Structure of axisymmetric mantle plumes, *J. Geophys. Res.* 98 (1993) 6829–6844.
- [4] G. Nolet, F.A. Dahlen, Wave front healing and the evolution of seismic delay times, *J. Geophys. Res.* 105 (2000) 19043–19054.
- [5] R. Montelli, G. Nolet, F.A. Dahlen, G. Masters, E.R. Engdahl, S.-H. Hung, Finite-frequency tomography reveals a variety of plumes in the mantle, *Science* 303 (2004) 338–343.
- [6] S. Goes, F. Cammarano, U. Hansen, Synthetic seismic signature of thermal mantle plumes, *Earth Planet. Sci. Lett.* 218 (2004) 403–419.
- [7] N.H. Sleep, Hotspots and mantle plumes: some phenomenology, *J. Geophys. Res.* 95 (1990) 6715–6736.
- [8] N. Ribe, U.R. Christensen, Three-dimensional modeling of plume–lithosphere interactions, *J. Geophys. Res.* 99 (1994) 669–682.
- [9] J. Phipps Morgan, W.J. Morgan, E. Price, Hotspot melting generates both hotspot volcanism and a hotspot swell? *J. Geophys. Res.* 100 (1995) 8045–8062.
- [10] B. Parsons, D. McKenzie, Mantle convection and the thermal structure of the plates, *J. Geophys. Res.* 83 (1978) 4485–4496.
- [11] S.D. King, Models of mantle viscosity, in: T.J. Ahrens (Ed.), *Mineral Physics and Crystallography: A Handbook of Physical Constants*, American Geophysical Union, Washington, DC, 1995, pp. 227–236.
- [12] V.S. Solomatov, Can hotter mantle have a larger viscosity? *Geophys. Res. Lett.* 23 (1996) 937–940.
- [13] V.S. Solomatov, R. El-Khozondar, V. Tikare, Grain size in the lower mantle: constraints from numerical modeling of grain growth in two-phase systems, *Phys. Earth Planet. Inter.* 129 (2002) 265–282.
- [14] S. Karato, S. Zhang, H.-R. Wenk, Superplasticity in Earth's lower mantle: evidence from seismic anisotropy and rock physics, *Science* 270 (1995) 458–461.
- [15] D. Yamazaki, T. Kato, E. Ohtani, M. Toriumi, Grain growth rates of MgSiO<sub>3</sub>-perovskite and periclase under lower mantle conditions, *Science* 274 (1996) 2052–2054.
- [16] V.S. Solomatov, Grain size-dependent viscosity convection and the thermal evolution of the Earth, *Earth Planet. Sci. Lett.* 191 (2001) 203–212.
- [17] A. Davaille, C. Jaupart, Transient high-Rayleigh-number thermal convection with large viscosity variations, *J. Fluid Mech.* 253 (1993) 141–166.
- [18] V.S. Solomatov, L.-N. Moresi, Scaling of time-dependent stagnant lid convection: application to small-scale convection on Earth and other terrestrial planets, *J. Geophys. Res.* 105 (2000) 21795–21817.
- [19] J. Korenaga, T.H. Jordan, Physics of multiscale convection in earth's mantle: onset of sublithospheric convection, *J. Geophys. Res.* 108 (B7) (2003) 2333, doi:10.1029/2002JB001760.
- [20] J. Korenaga, T.H. Jordan, Physics of multiscale convection in earth's mantle: evolution of sub-lithospheric convection, *J. Geophys. Res.* 109 (2004) B01405, doi:10.1029/2003B002464.
- [21] Q. Williams, The temperature contrast across D'', in: M. Gurnis, M.E. Wysession, E. Knittle, B.A. Buffett (Eds.), *The Core–Mantle Boundary Region*, American Geophysical Union, Washington, DC, 1998, pp. 73–81.
- [22] O.L. Anderson, The power balance at the core–mantle boundary, *Phys. Earth Planet. Inter.* 131 (2002) 1–17.
- [23] J. Huang, S. Zhong, J. van Hunen, Controls on sublithospheric small-scale convection, *J. Geophys. Res.* 108 (B8) (2003) 2405, doi:10.1029/2003JB002456.
- [24] S.E. Zaranek, E.M. Parmentier, The onset of convection in fluids with strongly temperature-dependent viscosity cooled from above with implications for planetary lithospheres, *Earth Planet. Sci. Lett.* 224 (2004) 371–386.
- [25] R.S. White, D. McKenzie, Mantle plumes and flood basal and flood basalts, *J. Geophys. Res.* 100 (1995) 17543–17585.
- [26] C.G. Farnetani, Excess temperature of mantle plumes: the role of chemical stratification across D'', *Geophys. Res. Lett.* 24 (1997) 11583–11586.
- [27] T. Lay, Q. Williams, E.J. Garnero, The core–mantle boundary layer and deep Earth dynamics, *Nature* 392 (1998) 461–468.
- [28] E.J. Garnero, Heterogeneity of the lowermost mantle, *Annu. Rev. Earth Planet. Sci.* 28 (2000) 509–537.
- [29] N.L. Montague, L.H. Kellogg, Numerical models of a dense layer at the base of the mantle and implications for the geodynamics of D'', *J. Geophys. Res.* 105 (2000) 11101–11114.
- [30] J.A. Whitehead Jr., D.S. Luther, Dynamics of laboratory diapir and plume models, *J. Geophys. Res.* 80 (1975) 705–717.

- [31] J. Korenaga, Mantle mixing and continental breakup magmatism, *Earth Planet. Sci. Lett.* 218 (2004) 463–473.
- [32] J. Crank, *The Mathematics of Diffusion*, 2nd edition, Oxford, New York, 1975.
- [33] W.J. Morgan, Convection plumes in the lower mantle, *Nature* 230 (1971) 42–43.
- [34] A.M. Jellinek, M. Manga, The influence of a chemical boundary layer on the fixity, spacing and lifetime of mantle plumes, *Nature* 418 (2002) 760–763.
- [35] B. Parsons, Causes and consequences of the relation between area and age of the ocean floor, *J. Geophys. Res.* 87 (1982) 289–302.
- [36] M.A. Richards, B.H. Hager, N.H. Sleep, Dynamically supported geoid highs over hotspots: observation and theory, *J. Geophys. Res.* 93 (1988) 7690–7708.
- [37] S. Karato, Seismic anisotropy in the deep mantle, boundary layers and the geometry of mantle convection, *PAGEOPH* 151 (1998) 565–587.
- [38] O.L. Anderson, *Equations of State of Solids for Geophysics and Ceramic Science*, Oxford, New York, 1995.
- [39] A.M. Dziewonski, D.L. Anderson, Preliminary reference Earth model, *Phys. Earth Planet. Inter.* 25 (1981) 297–356.